GDCh

Communication

Angewandte
Chemie
International Edition
www.angewandte.org

Nanomaterials **Hot Paper**

Enzyme-Triggered Assembly of Glycan Nanomaterials

Jacobus P. van Trijp[+], Nives Hribernik[+], Jia Hui Lim, Marlene C. S. Dal Colle,
Yadiel Vázquez Mena, Yu Ogawa,* and Martina Delbianco*

Abstract: A comprehensive molecular understanding of carbohydrate aggregation is key to optimize carbohydrate utilization and to engineer bioinspired analogues with tailored shapes and properties. However, the lack of well-defined synthetic standards has substantially hampered advances in this field. Herein, we employ a phosphorylation-assisted strategy to synthesize previously inaccessible long oligomers of cellulose, chitin, and xylan. These oligomers were subjected to enzyme-triggered assembly (ETA) for the on-demand formation of well-defined carbohydrate nanomaterials, including elongated platelets, helical bundles, and hexagonal particles. Cryo-electron microscopy and electron diffraction analysis provided molecular insights into the aggregation behavior of these oligosaccharides, establishing a direct connection between the resulting morphologies and the oligosaccharide primary sequence. Our findings demonstrate that ETA is a powerful approach to elucidate the intrinsic aggregation behavior of carbohydrates in nature. Moreover, the ability to access a diverse array of morphologies, expanded with a non-natural sequence, underscores the potential of ETA, coupled with sequence design, as a robust tool for accessing programmable glycan architectures.

Carbohydrates surpass all other biomacromolecules on Earth in both abundance and diversity.[1] In natural settings,

[*] J. P. van Trijp,[+] N. Hribernik,[+] M. C. S. Dal Colle, M. Delbianco
Department of Biomolecular Systems
Max Planck Institute of Colloids and Interfaces
Am Mühlenberg 1, 14476 Potsdam (Germany)
E-mail: martina.delbianco@mpikg.mpg.de

M. C. S. Dal Colle
Department of Chemistry and Biochemistry
Freie Universität Berlin
Arnimallee 22, 14195 Berlin (Germany)

J. H. Lim, Y. V. Mena, Y. Ogawa
Jia Hui Lim, Yadiel Vázquez Mena, Yu Ogawa
Univ. Grenoble Alpes
CNRS, CERMAV 38000 Grenoble (France)
E-mail: yu.ogawa@cermav.cnrs.fr

[+] These authors contributed equally

these biomolecules undergo self-assembly, leading to the formation of diverse morphologies that contribute to the development of hierarchical structural materials.[2] A comprehensive molecular understanding of these architectures is crucial for optimizing carbohydrate utilization and for engineering bioinspired analogues with tailored shapes and properties.[3] However, the molecular description of these complex architectures is hampered by a lack of standards with well-defined composition,[4] attributed to the intricacies of glycan synthesis and purification.[5] Consequently, the field of synthetic carbohydrate materials lags behind that of peptides[6] or nucleic acids,[7] whose structures and aggregation tendencies are better comprehended. To date, research on carbohydrate self-assembly has been centered on simple non-natural amphiphilic structures[8] or polydisperse polysaccharide systems.[9]

Synthetic oligosaccharides with well-defined sequences represent a valuable resource for elucidating the intricacies of glycan aggregation in nature[10] as well as important building blocks for the development of programmable glycan architectures.[11] These compounds can be synthesized through either chemical or enzymatic methods; however, both approaches encounter challenges as the glycan length increases.[12] Chemical synthesis of oligosaccharides heavily relies on protecting group strategies, which can be difficult to remove, leading to the formation of ill-defined aggregates.[13] Enzymatic synthesis bypasses the need of protecting groups, yet often lacks precise control over oligosaccharide length due to partial precipitation and aggregation of the chains during formation, finally leading to ill-defined mixtures of oligosaccharides.[14] Recent advances in solid support-based automated glycan assembly (AGA) have allowed for expedited and simplified synthesis of complicated glycan chains.[15] In particular, the incorporation of a solubilizing phosphate group at the end of the AGA process has successfully addressed the challenge of premature aggregation of a cellulose oligosaccharide.[16] The subsequent traceless removal of the phosphate group by alkaline phosphatase (ALP) triggered aggregation of cellulose oligomers into platelets.

Expanding upon these initial findings, we postulated that enzyme-triggered assembly (ETA) could serve as valuable strategy to 1) elucidate the intricate mechanisms underlying oligosaccharide aggregation and 2) induce the on-demand formation of carbohydrate nanomaterials (Figure 1). Herein, we showcase the efficacy of ETA in shedding light on the assembly of well-defined long oligomers, representative of natural cellulose, chitin, and xylan. ETA enables us to initiate the aggregation of both natural and non-natural oligosacchar-
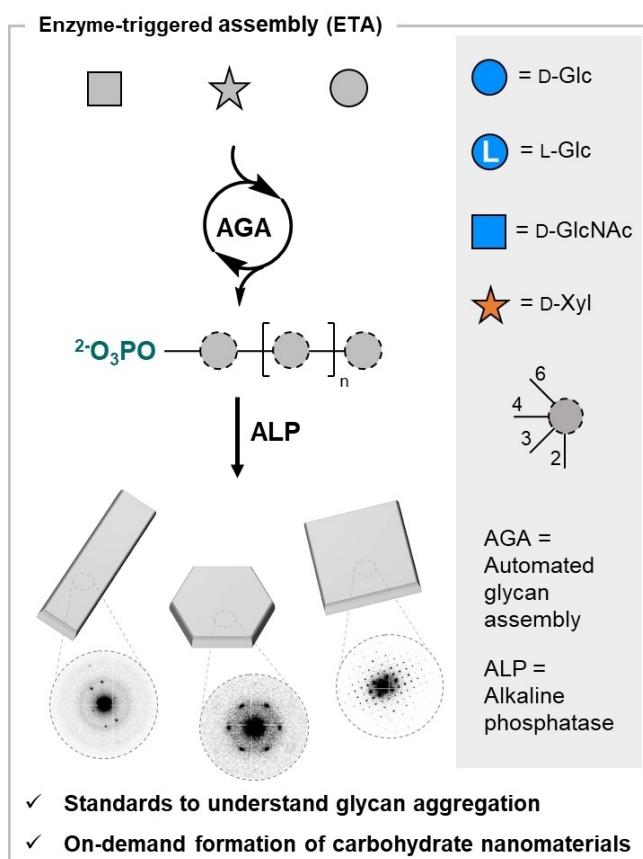
Figure 1. Enzyme-triggered assembly (ETA) as strategy to unveil the mechanism of oligosaccharide aggregation in nature and produce carbohydrate nanomaterials on-demand. Monosaccharide residues used in this work represented following the Symbol Nomenclature for Glycans (SNFG).[17]

ide sequences and explore the chemical space accessible with synthetic carbohydrate assemblies.

We first explored the ETA of cellulose oligosaccharides of different length. Non-phosphorylated cellulose oligomers proved insoluble in aqueous environment already at the hexasaccharide level, generating crystalline platelets, limiting access to longer analogues.[10] Thus, these oligomers are ideal substrates to evaluate the potential of the ETA approach.

ETA requires the following steps: AGA of the target carbohydrate sequence, solid-phased phosphorylation,[18] post-AGA steps (i.e. methanolysis and hydrogenolysis) to liberate the phosphorylated glycan, and ALP-mediated dephosphorylation.[16] The latter releases the native glycan, triggering its self-assembly into a nanomaterial.

The cellulose backbones were prepared by AGA with full control over the oligomer length (see SI). Phosphorylation was strategically planned at the non-reducing terminal C-4 hydroxyl group to circumvent the instability issues associated with primary phosphate esters (i.e. at C-6) during the methanolysis step in post-AGA,[18] while still allowing for rapid dephosphorylation. With this strategy, the phosphorylated cellulose 6-mer (**P-A$_6$**) was obtained in a 47% overall yield (Figure 2A), confirming the chemical stability of the phosphate group during the post-AGA step. Next, we targeted the

synthesis of the monophosphorylated 10-mer and 12-mer (**P-A$_{10}$** and **P-A$_{12}$**). Optimization of hydrogenolysis and purification steps was necessary to ensure the efficient isolation of the target compound. Centrifugation, instead of filtration, proved effective in removing the majority of the Pd/C catalyst, preventing clogging issues. Size-exclusion column chromatography afforded the pure **P-A$_{10}$** and **P-A$_{12}$** in 6% and 38% yield, respectively (Figure 2A, the relative low yield for **P-A$_{10}$** was attributed to issues during the AGA step, see SI). Following the same procedure, the monophosphorylated cellulose 18-mer (**P-A$_{18}$**) was isolated in 8% yield. All oligomers formed transparent and stable suspensions in water. In contrast, the monophosphorylated cellulose 21-mer (**P-A$_{21}$**) showed substantial aggregation that drastically reduced its isolated yield (1%), identifying the length limiting value for this approach.

X-ray diffraction (XRD) analysis revealed the cellulose II type of aggregation for all monophosphorylated cellulose derivatives in the solid state upon drying (Figure S4). As the oligomer length increased, a noticeable lower-angle shift of the 1–10 reflection was observed, indicating the formation of a cellulose II hydrate allomorph.[19] Thus, the presence of phosphate groups destabilized the intermolecular interactions between the hydrophobic ring stacking in the cellulose II crystals. Cryo-TEM analysis of the phosphorylated oligomers in aqueous solutions showed the presence of small poorly crystalline colloidal aggregates for **P-A$_{10}$**, **P-A$_{12}$** and **P-A$_{18}$** (Figure S7, S8, S9 and S10), while no aggregates were observed for **P-A$_6$** (Figure S5). We hypothesize that, while the hydrophilic phosphate moiety impeded extended regular organization, some intermolecular interactions, such as hydrophobic stacking of the glycosidic rings, may still occur when the saccharide part reaches a certain size.

Next, we studied the formation of cellulose-based nanomaterials via ETA. First, we proved that ALP performed efficiently also on a secondary position (C-4). Dephosphorylation using ALP proceeded smoothly for **P-A$_6$**, with quantitative conversion to the native **A$_6$** as confirmed by MALDI-TOF analysis (Figure S11). The same procedure was applied to longer phosphorylated cellulose analogues, releasing the native cellulose oligomers of defined lengths (**A$_{10}$**, **A$_{12}$**, **A$_{18}$**, **A$_{21}$**) and allowing us to investigate the effect of chain length on cellulose assembly (Figure 2B). Upon ETA of a 2.0% (w/w) solution, **A$_6$** formed rigid rod-like platelets that precipitated out of solution. In contrast, when ETA was performed with longer oligosaccharides (**P-A$_{10}$**, **P-A$_{12}$**, **P-A$_{18}$**), we triggered the formation of colloidal thin fibrillar structures (Figure S23 and S24). The assemblies obtained for **A$_{10}$**, **A$_{12}$** and **A$_{18}$** were significantly larger than the phosphorylated counterparts, confirming the crystal growth triggered by ETA (Figure S21). Electron diffraction (ED) analysis revealed that all crystals adopted the cellulose II type molecular packing (Figure S13–S20), with the oligomers aligned in an antiparallel manner along the fiber thickness direction (Figure 2C). However, the morphology of the assemblies was dramatically affected by oligomer chain length, with longer chains resulting in thinner and less defined in shape aggregates.

To verify whether the kinetics of the dephosphorylation reaction influenced self-assembly and potentially the final
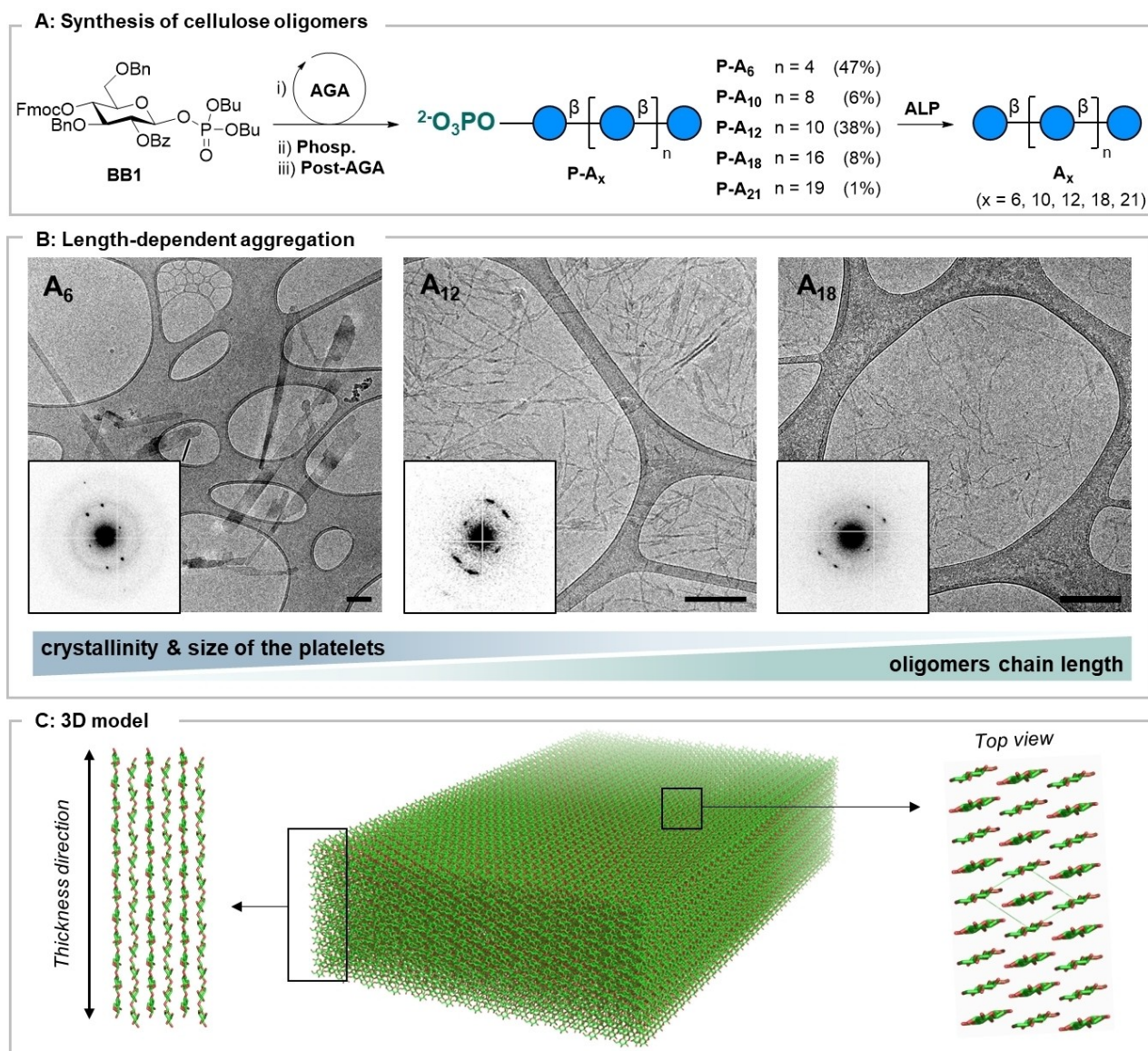
Figure 2. (A) AGA of cellulose analogues **P-A₆**, **P-A₁₀**, **P-A₁₂**, **P-A₁₈** and **P-A₂₁** using building block **BB1** and ALP mediated dephosphorylation. (B) Cryo-TEM images and electron diffraction of crystallites of **A₆**, **A₁₂** and **A₁₈** (scale bars 200 nm). (C) Three-dimensional molecular model of the platelets composed of cellulose oligomers arranged in antiparallel fashion according to the cellulose II crystal structure.

assembly morphologies, we analyzed the two steps of the ETA process (Figure 3, S25–27). *In situ* ^{31}P NMR spectroscopy revealed that the dephosphorylation step was completed within 12 min after addition of ALP. In contrast, cryo-TEM detected non-crystalline aggregation with only a small fraction of crystalline platelets even after 1 h of reaction time. The formation of mature crystalline A_6 platelets was observed after 24 h, demonstrating that the kinetics of self-assembly are not affected by the dephosphorylation step. The slow crystallization kinetics resulted in extended highly ordered structures for A_6. The initial concentrations of **P-A₆**, had a bigger impact on the assembly morphology, with small platelets that formed twisted bundles upon drying at 0.1 % (w/w) and large rigid platelets at 2.0 % (w/w) (Figure S22).

Similar differences in the rate of dephosphorylation and assembly were observed for **P-A₁₂**, even though, fibrillar aggregates similar to the mature fibrils were visualized already after 1 h (Figure S26). These aggregates were shorter than the mature ones, indicating the continuous growth of aggregates after initial fibril formation (Figure S26). Upon ETA, the poor solubility of the A_{12} oligomers at the dephosphorylated stage contributed to the faster assembly. This tendency, exacerbated for A_{18}, could be connected to the formation of multiple irregular crystallites. For these long analogues, no substantial differences in the size of the assemblies were observed when ETA was performed at different concentrations (Figure S23 and S24). Taken together, these observations demonstrated that ETA reveals the intrinsic aggregation behavior of
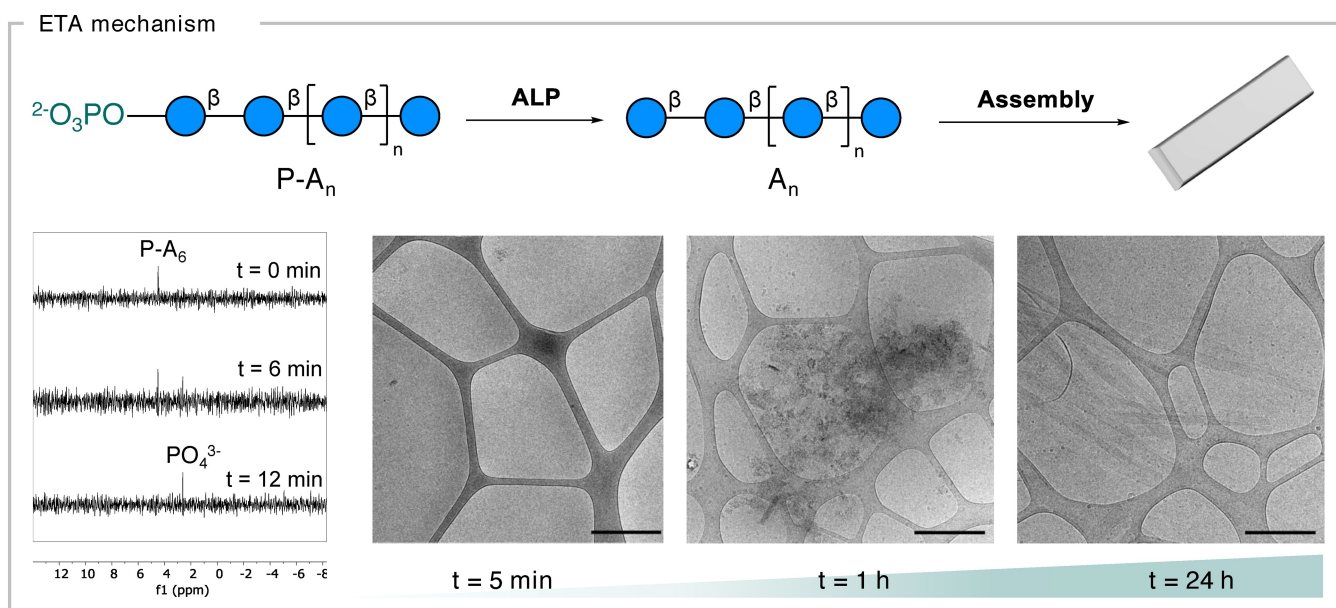
Figure 3. Schematic representation of ETA exemplified for a cellulose oligomer. The process includes an ALP mediated dephosphorylation step that releases the native glycan and trigger its assembly into a nanomaterial. ^{31}P NMR analysis showing that the first step of the ETA process (i.e. dephosphorylation) is completed within 12 min. In contrast, TEM analysis showed much slower kinetics for the assembly step, with mature aggregates formed after 24 h (scale bar 500 nm). These results are exemplified for **P-A$_6$**, the same analysis for **P-A$_{12}$** can be found in Figure S26.

oligosaccharides and it is not influenced by the dephosphorylation step.

We then extended the application of ETA to investigate the aggregation of other glycans and explore the chemical space achievable with synthetic glycan assemblies. Besides cellulose, chitin[20] (β-1,4-*N*-acetylglucosamine) and xylan[21] (β-1,4-xylose) are abundant natural polysaccharides known to form nanoarchitectures. Similar to cellulose oligomers, the poor solubility of chitin and xylan oligomers has posed challenges to their synthesis,[22,14b] thereby hindering their utilization for the production of well-defined, tailor-made nanomaterials. We synthesized a monophosphorylated chitin 6-mer (**P-N$_6$**), following AGA conditions developed for non-phosphorylated analogs.[22–23] Compound **P-N$_6$** was isolated in 14% yield (Figure 4A). In contrast to the phosphorylated cellulose structures, **P-N$_6$** showed high crystallinity in powder X-ray diffraction (Figure S28) and reduced solubility in water (<4 mg/mL) compared to the non-phosphorylated chitin 6-mer (13–17 mg/mL).[24] However, AFM and TEM analysis of **P-N$_6$** showed no ordered assemblies with well-defined morphology (Figure S29). ETA afforded **N$_6$**, which was precipitated with isopropanol and diluted with water right before analysis (see Supporting Information for detailed procedure). Fibrous assemblies that came together in left-handed twists were observed in AFM and (cryo)-TEM (Figure 4A and S30–32). ED analysis showed that **N$_6$** was crystallized into the α-chitin allomorph,[25] with the oligomer chains aligned in an antiparallel manner along the transverse direction of the fibers (Figure 4A).

Next, we turned our attention to xylan.[21b] Enzymatically synthesized xylan polydispersed oligomers were shown to form solid nanoparticles, with the insoluble fraction detected to be around 18 monosaccharide units.[14a] The limited solubility of xylans could be alleviated with permanent chemical modifications, such as methylation, simplifying their synthesis, but precluding comparison to natural glycans.[14b] Thus, we set out to synthesize phosphorylated xylan oligomers to study their properties and self-assembly upon ETA. As narrowness of molecular weight distribution decreases water solubility,[26] we targeted a hexamer (**P-Y$_6$**) and a dodecamer (**P-Y$_{12}$**). **P-Y$_6$** and **P-Y$_{12}$** were synthesized in 10% and 8% yield, respectively (Figure 4B). XRD profiles showed amorphous features for both derivatives (Figure S33), which appear highly soluble in water. After ETA, poorly defined aggregates were observed for **Y$_6$** (Figure S34), indicating that this chain length is insufficient for the formation of ordered assembly. In contrast, TEM observation of **Y$_{12}$** precipitated in isopropanol revealed presence of hexagonal assemblies, along with a minor part of the material forming right-handed twist-like assemblies (Figure S35). ED of the hexagonal assemblies identified the xylan hydrate crystal structure, where the oligomers were packed in a hexagonal unit cell and aligned along their thickness direction[27] (Figure 4B and S36).

To broaden further the scope of nanomaterial morphologies achievable through ETA, we explored the assembly of a non-natural glycan sequence. Recently, we demonstrated that chemical modifications in the core of cellulose chains could be leveraged to access different morphologies.[11b] By incorporating an enantiomeric residue (i.e. L-glucose) in the middle of a D-glucose sequence (**A$_3$LA$_4$**), we altered the packing of the molecules within the crystal to generate a rare cellulose IV$_{II}$ allomorph characterized by crystals with a distinctive square geometry.[28] We synthesized the phosphorylated analogue **P-A$_3$LA$_4$** in a 13% overall yield (Figure 4C). The presence of the
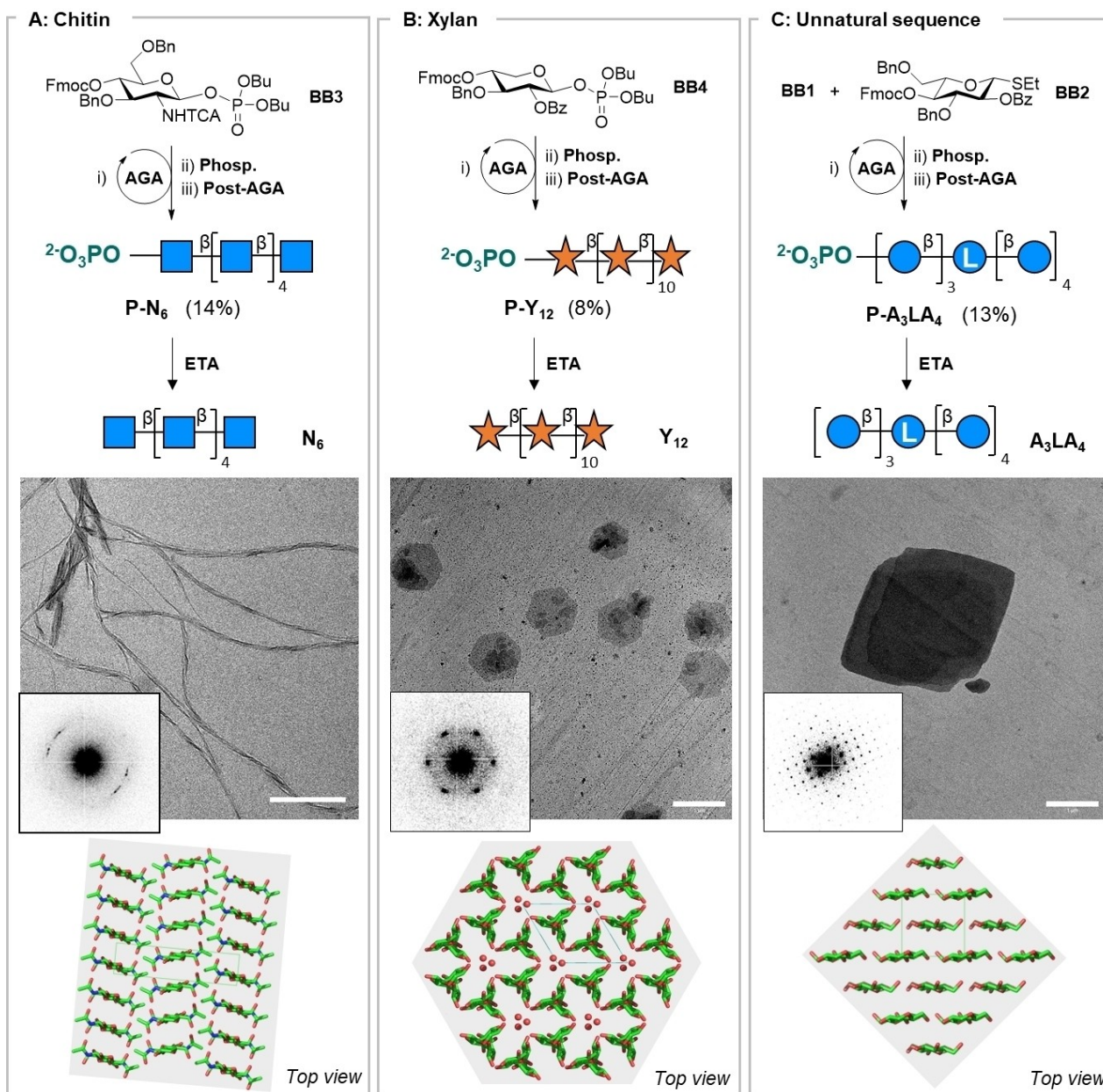
Figure 4. Synthesis of phosphorylated oligosaccharides and ETA to trigger the formation of nanomaterials based on (A) chitin, (B) xylan, and (C) a glycan unnatural sequence. Conditions used for each ETA process can be found in the Supporting Information section 2.1. General methods. Upon ETA, each sample was characterized with (cryo)-TEM and ED (scale bars: 1 μm). For each assembly, the schematic model (top view) is reported. The crystallographic information is summarized in Table S1.

phosphate moiety disrupted crystalline organization (Figure S37), resulting in a substantial increase in water solubility compared to the non-phosphorylated counterpart. Upon ETA, the typical cellulose IV_{II} square-like geometry was observed in TEM. The high water solubility of **P-A₃LA₄** allowed us to conduct ETA at 2.0 % (w/w), leading to square and rectangular crystals with lateral dimensions exceeding 1 μm (Figure 4C and S38), in contrast to previously obtained self-assembled aggregates of 50–200 nm.[11b] The resolution of the electron diffraction was much higher than in previously studied cellulose IV_{II} crystals, being well beyond 1 Å (Figure S39 and S40). Such resolution offers opportunities to solve the structure

of cellulose IV_{II}, a lesser-known cellulose allomorph, at atomic resolution based on single crystal electron crystallography.

In conclusion, we successfully synthesized previously inaccessible long oligomers of cellulose, chitin, and xylan taking advantage of a phosphorylation-assisted strategy. A single phosphate ester installed at the non-reducing terminus of aggregating oligosaccharide sequences allowed us to readily disperse in aqueous solution oligomers with length up to 21-mer (for non-phosphorylated cellulose oligomers the synthetic limit is 6-mer[10]). We speculate that this approach could be further expanded including multiple phosphate esters,[16] pushing the limit of synthetic polysaccharide chemistry.

Through ETA, we induced the formation of well-defined carbohydrate materials, whose morphology is encoded in the oligosaccharide primary sequence. These samples served as models to investigate the aggregation of natural polysaccharides[2a] and shed light on the intrinsic chain length dependent aggregation behavior of cellulose molecules. Cryo-(EM) and ED analysis provided molecular insights into the arrangement of the oligosaccharide chains within cellulose, chitin, and xylan nanomaterials. This behavior was exploited to access a diverse array of morphologies, including elongated platelets, helical bundles, as well as hexagonal particles. The collection of nanomaterials was expanded with a non-natural glycan sequence, opening the way to a square-like geometry. These findings underscore the potential of ETA, coupled with sequence design, as a robust tool for accessing programmable glycan architectures on-demand. Such carbohydrate-based materials expand the portfolio of nanostructures achievable with other biopolymers such as peptides[29] and nucleic acids,[30] with implications in materials science and nanotechnology.[31,3c]

Supporting Information

The authors have cited additional references within the Supporting Information.[32]

Notes

The authors declare no competing financial interest.

Author Contributions

Acknowledgements

Conflict of Interest

The authors declare no conflict of interest.

Data Availability Statement

All experimental details regarding building block synthesis, AGA, NMR, XRD, TEM and AFM are reported in the Supporting Information. Raw data for NMR analysis, XRD, cryo-TEM, and ED analysis can be downloaded from https://doi.org/10.17617/3.IQSPTF, Edmond.

Keywords: Glycans · Nanomaterials · Cryo-TEM

[1] A. Varki, R. D. Cummings, J. D. Esko, P. Stanley, G. W. Hart, M. Aebi, D. Mohnen, T. Kinoshita, N. H. Packer, J. H. Prestegard, R. L. Schnaar, P. H. Seeberger, in *Essentials of Glycobiology*, Cold Spring Harbor Laboratory Press by the Consortium of Glycobiology Editors, La Jolla, California. Published by Cold Spring Harbor Laboratory Press, Cold Spring Harbor, New York. All rights reserved., Cold Spring Harbor (NY), **2022**.

[2] a) S. Pérez, M. Kouwijzer, in *Carbohydrates: Structures, Syntheses and Dynamics* (Ed.: P. Finch), Springer Netherlands, Dordrecht, **1999**, pp. 258–293; b) P. Fratzl, R. Weinkamer, *Prog. Mater. Sci.* **2007**, *52*, 1263–1334; c) R. J. Moon, A. Martini, J. Nairn, J. Simonsen, J. Youngblood, *Chem. Soc. Rev.* **2011**, *40*, 3941–3994; d) B. Thomas, M. C. Raj, A. K. B, R. M. H, J. Joy, A. Moores, G. L. Drisko, C. Sanchez, *Chem. Rev.* **2018**, *118*, 11575–11625.

[3] a) M. Delbianco, P. H. Seeberger, *Mater. Horiz.* **2020**, *7*, 963–969; b) L. Su, Y. Feng, K. Wei, X. Xu, R. Liu, G. Chen, *Chem. Rev.* **2021**, *121*, 10950–11029; c) S. Djalali, N. Yadav, M. Delbianco, *Nat. Rev. Mater.* **2024**.

[4] R. J. Woods, *Chem. Rev.* **2018**, *118*, 8005–8024.

[5] a) T. J. Boltje, T. Buskas, G.-J. Boons, *Nat. Chem.* **2009**, *1*, 611–622; b) P. H. Seeberger, *Nat. Chem. Biol.* **2009**, *5*, 368–372; c) C. J. Gray, L. G. Migas, P. E. Barran, K. Pagel, P. H. Seeberger, C. E. Eyers, G.-J. Boons, N. L. B. Pohl, I. Compagnon, G. Widmalm, S. L. Flitsch, *J. Am. Chem. Soc.* **2019**, *141*, 14463–14479.

[6] a) S. Abb, L. Harnau, R. Gutzler, S. Rauschenbach, K. Kern, *Nat. Commun.* **2016**, *7*, 10335; b) A. Levin, T. A. Hakala, L. Schnaider, G. J. L. Bernardes, E. Gazit, T. P. J. Knowles, *Nat. Chem. Rev.* **2020**, *4*, 615–634; c) F. Sheehan, D. Sementa, A. Jain, M. Kumar, M. Tayarani-Najjaran, D. Kroiss, R. V. Ulijn, *Chem. Rev.* **2021**, *121*, 13869–13914; d) N. J. Sinha, M. G. Langenstein, D. J. Pochan, C. J. Kloxin, J. G. Saven, *Chem. Rev.* **2021**, *121*, 13915–13935; e) C. Yang, F. Sesterhenn, J. Bonet, E. A. van Aalen, L. Scheller, L. A. Abriata, J. T. Cramer, X. Wen, S. Rosset, S. Georgeon, T. Jardetzky, T. Krey, M. Fussenegger, M. Merkx, B. E. Correia, *Nat. Chem. Biol.* **2021**, *17*, 492–500; f) J. Dodd-o, A. Roy, Z. Siddiqui, R. Jafari, F. Coppola, S. Ramasamy, A. Kolloli, D. Kumar, S. Kaundal, B. Zhao, R. Kumar, A. S. Robang, J. Li, A.-R. Azizogli, V. Pai, A. Acevedo-Jake, C. Heffernan, A. Lucas, A. C. McShan, A. K. Paravastu, B. V. V. Prasad, S. Subbian, P. Král, V. Kumar, *Nat. Commun.* **2024**, *15*, 1142.

[7] a) M. R. Jones, N. C. Seeman, C. A. Mirkin, *Science* **2015**, *347*, 1260901; b) Y. Hu, C. M. Niemeyer, *Adv. Mater.* **2019**, *31*,

1806294; c) Y. Dong, C. Yao, Y. Zhu, L. Yang, D. Luo, D. Yang, *Chem. Rev.* **2020**, *120*, 9420–9481; d) T. Tian, T. Zhang, S. Shi, Y. Gao, Y. Cai, Y. Lin, *Nat. Protoc.* **2023**, *18*, 1028–1055; e) P. Zhan, A. Peil, Q. Jiang, D. Wang, S. Mousavi, Q. Xiong, Q. Shen, Y. Shang, B. Ding, C. Lin, Y. Ke, N. Liu, *Chem. Rev.* **2023**, *123*, 3976–4050.

[8] a) A. Brito, S. Kassem, R. L. Reis, R. V. Ulijn, R. A. Pires, I. Pashkuleva, *Chem* **2021**, *7*, 2943–2964; b) V. I. B. Castro, A. R. Araújo, F. Duarte, A. Sousa-Franco, R. L. Reis, I. Pashkuleva, R. A. Pires, *ACS Appl. Mater. Interfaces* **2023**, *15*, 29998–30007; c) B. Wang, S. Liu, H. Li, W. Dong, H. Liu, J. Zhang, C. Tian, S. Dong, *Angew. Chem. Int. Ed.* **2024**, *63*, e202309140.

[9] a) B.-S. Kim, D.-J. Hong, J. Bae, M. Lee, *J. Am. Chem. Soc.* **2005**, *127*, 16333–16337; b) K. Petzold-Welcke, K. Schwikal, S. Daus, T. Heinze, *Carbohydr. Polym.* **2014**, *100*, 80–88; c) Y. Fan, Y. Liu, Y. Wu, F. Dai, M. Yuan, F. Wang, Y. Bai, H. Deng, *Int. J. Biol. Macromol.* **2021**, *192*, 1240–1255.

[10] G. Fittolani, D. Vargová, P. H. Seeberger, Y. Ogawa, M. Delbianco, *J. Am. Chem. Soc.* **2022**, *144*, 12469–12475.

[11] a) B. van Genabeek, B. A. G. Lamers, C. J. Hawker, E. W. Meijer, W. R. Gutekunst, B. V. K. J. Schmidt, *J. Polym. Sci.* **2021**, *59*, 373–403; b) N. Hribernik, D. Vargová, M. C. S. Dal Colle, J. H. Lim, G. Fittolani, Y. Yu, J. Fujihara, K. Ludwig, P. H. Seeberger, Y. Ogawa, M. Delbianco, *Angew. Chem. Int. Ed.* **2023**, *62*, e202310357.

[12] a) G. Fittolani, T. Tyrikos-Ergas, D. Vargová, M. A. Chaube, M. Delbianco, *Beilstein J. Org. Chem.* **2021**, *17*, 1981–2025; b) S. Wang, Y. Yang, Q. Zhu, G.-Q. Lin, B. Yu, *Curr. Opin. Chem. Biol.* **2022**, *69*, 102154.

[13] Y. Yu, S. Gim, D. Kim, Z. A. Arnon, E. Gazit, P. H. Seeberger, M. Delbianco, *J. Am. Chem. Soc.* **2019**, *141*, 4833–4838.

[14] a) P. J. Smith, T. M. Curry, J.-Y. Yang, W. J. Barnes, S. J. Ziegler, A. Mittal, K. W. Moremen, W. S. York, Y. J. Bomble, M. J. Peña, B. R. Urbanowicz, *ACS Materials Au* **2022**, *2*, 440–452; b) I. Álvarez-Martínez, C. Ruprecht, D. Senf, H.-t. Wang, B. R. Urbanowicz, F. Pfrengle, *Chem. Eur. J.* **2023**, *29*, e202203941.

[15] a) A. A. Joseph, A. Pardo-Vargas, P. H. Seeberger, *J. Am. Chem. Soc.* **2020**, *142*, 8561–8564; b) J.-Y. Huang, M. Delbianco, *Synthesis* **2022**, *55*, 1337–1354.

[16] E. T. Sletten, G. Fittolani, N. Hribernik, M. C. S. Dal Colle, P. H. Seeberger, M. Delbianco, *ACS Cent. Sci.* **2023**.

[17] A. Varki, R. D. Cummings, M. Aebi, N. H. Packer, P. H. Seeberger, J. D. Esko, P. Stanley, G. Hart, A. Darvill, T. Kinoshita, J. J. Prestegard, R. L. Schnaar, H. H. Freeze, J. D. Marth, C. R. Bertozzi, M. E. Etzler, M. Frank, J. F. Vliegenthart, T. Lütteke, S. Perez, E. Bolton, P. Rudd, J. Paulson, M. Kanehisa, P. Toukach, K. F. Aoki-Kinoshita, A. Dell, H. Narimatsu, W. York, N. Taniguchi, S. Kornfeld, *Glycobiology* **2015**, *25*, 1323–1324.

[18] E. T. Sletten, J. Danglad-Flores, S. Leichnitz, A. Abragam Joseph, P. H. Seeberger, *Carbohydr. Res.* **2022**, *511*, 108489.

[19] K. Kobayashi, S. Kimura, E. Togawa, M. Wada, *Carbohydr. Polym.* **2011**, *86*, 975–981.

[20] a) G. A. F. Roberts, in *Chitin Chemistry* (Ed.: G. A. F. Roberts), Macmillan Education UK, London, **1992**, pp. 1–53; b) N. Yan, X. Chen, *Nature* **2015**, *524*, 155–157.

[21] a) H. V. Scheller, P. Ulvskov, *Annu. Rev. Plant Biol.* **2010**, *61*, 263–289; b) T. M. Curry, M. J. Peña, B. R. Urbanowicz, *Cell Surf* **2023**, *9*, 100101.

[22] T. Tyrikos-Ergas, V. Bordoni, G. Fittolani, M. A. Chaube, A. Grafmüller, P. H. Seeberger, M. Delbianco, *Chemistry* **2021**, *27*, 2321–2325.

[23] G. Fittolani, S. Djalali, M. A. Chaube, T. Tyrikos-Ergas, M. C. S. Dal Colle, A. Grafmüller, P. H. Seeberger, M. Delbianco, *Org. Biomol. Chem.* **2022**, *20*, 8228–8235.

[24] Y. Yu, T. Tyrikos-Ergas, Y. Zhu, G. Fittolani, V. Bordoni, A. Singhal, R. J. Fair, A. Grafmüller, P. H. Seeberger, M. Delbianco, *Angew. Chem. Int. Ed.* **2019**, *58*, 13127–13132.

[25] P. Sikorski, R. Hori, M. Wada, *Biomacromolecules* **2009**, *10*, 1100–1105.

[26] R. L. Whistler, in *Carbohydrates in Solution, Vol. 117*, AMERICAN CHEMICAL SOCIETY, **1973**, pp. 242–255.

[27] I. A. Nieduszynski, R. H. Marchessault, *Biopolymers* **1972**, *11*, 1335–1344.

[28] a) A. D. French, S. Pérez, V. Bulone, T. Rosenau, D. Gray, in *Encyclopedia of Polymer Science and Technology*, pp. 1–69; b) A. Buleon, H. Chanzy, *Journal of Polymer Science: Polymer Physics Edition* **1980**, *18*, 1209–1217; c) P. Zugenmaier, *Cellulose*, 1 ed., Springer Berlin, Heidelberg, **2008**, pp. 101–171.

[29] a) B. J. Pepe-Mooney, R. Fairman, *Curr. Opin. Struct. Biol.* **2009**, *19*, 483–494; b) J. Gao, J. Zhan, Z. Yang, *Adv. Mater.* **2020**, *32*, 1805798; c) G. Ghosh, R. Barman, A. Mukherjee, U. Ghosh, S. Ghosh, G. Fernández, *Angew. Chem. Int. Ed.* **2022**, *61*, e202113403; d) T. Li, X. M. Lu, M. R. Zhang, K. Hu, Z. Li, *Bioact Mater* **2022**, *11*, 268–282; e) S. Shabani, S. Hadjigol, W. Li, Z. Si, D. Pranantyo, M. B. Chan-Park, N. M. O'Brien-Simpson, G. G. Qiao, *Nat. Rev. Bioeng.* **2024**.

[30] a) N. C. Seeman, *Nature* **2003**, *421*, 427–431; b) L. N. Green, H. K. K. Subramanian, V. Mardanlou, J. Kim, R. F. Hariadi, E. Franco, *Nat. Chem.* **2019**, *11*, 510–520; c) L. Fang, C. Shi, Y. Wang, Z. Xiong, Y. Wang, *J. Nanobiotechnol.* **2023**, *21*, 290; d) C. Rossi-Gendron, F. El Fakih, L. Bourdon, K. Nakazawa, J. Finkel, N. Triomphe, L. Chocron, M. Endo, H. Sugiyama, G. Bellot, M. Morel, S. Rudiuk, D. Baigl, *Nat. Nanotechnol.* **2023**, *18*, 1311–1318.

[31] a) Y. Habibi, L. A. Lucia, O. J. Rojas, *Chem. Rev.* **2010**, *110*, 3479–3500; b) B. Frka-Petesic, T. G. Parton, C. Honorato-Rios, A. Narkevicius, K. Ballu, Q. Shen, Z. Lu, Y. Ogawa, J. S. Haataja, B. E. Droguet, R. M. Parker, S. Vignolini, *Chem. Rev.* **2023**, *123*, 12595–12756.

[32] a) E. S. Gardiner, A. Sarko, *Can. J. Chem.* **1985**, *63*, 173–180; b) P. Langan, Y. Nishiyama, H. Chanzy, *Biomacromolecules* **2001**, *2*, 410–416; c) M. Gude, J. Ryf, P. D. White, *Lett. Pept. Sci.* **2002**, *9*, 203–206; d) S. Eller, M. Collot, J. Yin, H. S. Hahm, P. H. Seeberger, *Angew. Chem. Int. Ed.* **2013**, *52*, 5858–5861; e) M. Hurevich, J. Kandasamy, B. M. Ponnappa, M. Collot, D. Kopetzki, D. T. McQuade, P. H. Seeberger, *Org. Lett.* **2014**, *16*, 1794–1797; f) D. Schmidt, F. Schuhmacher, A. Geissner, P. H. Seeberger, F. Pfrengle, *Chem. Eur. J.* **2015**, *21*, 5709–5713; g) P. Dallabernardina, F. Schuhmacher, P. H. Seeberger, F. Pfrengle, *Org. Biomol. Chem.* **2016**, *14*, 309–313; h) K. Le Mai Hoang, A. Pardo-Vargas, Y. Zhu, Y. Yu, M. Loria, M. Delbianco, P. H. Seeberger, *J. Am. Chem. Soc.* **2019**, *141*, 9079–9086.